5-1994

Observations of gamma-ray bursts by COMPTEL

L O. Hanlon
ESTEC

K Bennett
ESTEC

W Collmar
Max-Planck-Institut für extraterrestriche Physik

A Connors
University of New Hampshire - Main Campus

R Diehl
Max-Planck-Institut für extraterrestriche Physik

See next page for additional authors

Astron. Astrophys. 285, 161–178 (1994)

ASTRONOMY AND ASTROPHYSICS

Observations of gamma–ray bursts by COMPTEL

L.O. Hanlon[4], K. Bennett[4], W. Collmar[1], A. Connors[3], R. Diehl[1], R. van Dijk[2*], J. Greiner[1], J.W. den Herder[2], W. Hermsen[2], R.M. Kippen[3], L. Kuiper[2], M. McConnell[3], J. Ryan[3], V. Schönfelder[1], H. Steinle[1], A. Strong[1], M. Varendorff[3], O.R. Williams[4], and C. Winkler[4]

[1] Max-Planck-Institut für Extraterrestrische Physik, D-85748 Garching, Germany
[2] SRON-Leiden, P.O. Box 9504, NL-2300 RA Leiden, The Netherlands
[3] University of New Hampshire, Institute for the Studies of Earth, Oceans and Space, Durham NH 03824, USA
[4] Astrophysics Division, Space Science Department of ESA/ESTEC, NL-2200 AG Noordwijk, The Netherlands

Received 27 July 1993 / Accepted 6 November 1993

Abstract. During the first year of operation, 22 cosmic gamma–ray bursts were detected within the field of view of the COMPTEL instrument on board the *Compton* Gamma Ray Observatory. Spectra and time histories for the strongest of these bursts have been obtained from both the main instrument (0.75–30 MeV) and the burst modules (0.3–10 MeV).

The deconvolved photon spectra for the majority of bursts are fit by a single power law model with spectral index between -1.6 and -2.8. One strong burst, GRB 910814, exhibited significant curvature and could not be fit by a single power law model. A broken power law model with a break in slope at ~ 2 MeV is a good fit to the time averaged spectrum of this burst. There is evidence in the COMPTEL data, at the 2.8σ level, for a changing break energy in GRB 910814, from above 2 MeV to below 1 MeV during the first 9 s of the burst. This is the first report of a time dependent turnover at MeV energies in the spectrum of a gamma–ray burst.

GRB 910503 was the only burst in our sample which exhibited significant hard to soft evolution. We show that our observations of spectral evolution in the sample of data examined do not conflict with the assertion by SMM that hard to soft evolution is a characteristic feature of MeV emission from gamma–ray bursts.

The strongest bursts were located using COMPTEL's independent imaging capability and location maps for each imaged burst are presented. The intersection of the COMPTEL locations with triangulation arcs derived from the Interplanetary Network (IPN) results in a smaller error box for counterpart searchers to examine.

Key words: gamma–ray bursts – space vehicles

Send offprint requests to: L.O. Hanlon

* Also: Astronomical Institute, University of Amsterdam, Kruislaan 403, NL-1098 SJ, Amsterdam, The Netherlands

1. Introduction

COMPTEL is an imaging gamma–ray telescope on board the *Compton* Gamma Ray Observatory (CGRO), operating in the energy range 0.75 – 30 MeV. The primary scientific goal of COMPTEL is to perform the first all-sky survey in this energy region. One of its secondary scientific objectives is the study of gamma–ray transients, including gamma–ray bursts (GRBs).

The instrument consists of an upper layer of seven detectors (total area 4188 cm^2), made from the low-Z liquid scintillator material NE213A along with a lower layer of fourteen NaI cells (total area 8620 cm^2). Two separate modes of operation are employed by COMPTEL for the detection of GRBs.

The "double scatter" (or "telescope") mode, which is the normal imaging mode of the telescope, is used to produce images, spectra (0.75 – 30 MeV) and lightcurves of bursts which occur within the field of view (FOV). Briefly, an incoming photon undergoes Compton scattering in the upper D-1 detector layer and then travels ~ 1.5 m to the lower D-2 detector array where it interacts a second time. This constitutes an ideal COMPTEL event. Non-ideal events, for example, an incoming photon undergoing bremsstrahlung and then interacting in the D2 layer, are accounted for in the point-spread function of the instrument.

The measured quantities per event include the locations and energy deposits of these interactions in D1 and D2, the pulse shape of the interaction in D1, the absolute time ($125\mu s$ accuracy) of the event and the time – of – flight of the scattered photon from the upper to the lower detector. Measurement of the pulse shape in D1 and the time – of – flight between D1 and D2 permits the rejection of various types of background events, including neutron induced events. The possible arrival directions for completely absorbed events lie on a circle, called the event circle, with radius $\bar{\phi}$ around the direction of the scattered gamma–ray, such that:

$$\cos(\bar{\phi}) = 1 - \frac{mc^2}{E_2} + \frac{mc^2}{E_1 + E_2} \qquad (1)$$

where mc^2 is the electron rest mass energy and E_1 and E_2 are the energy deposits of the gamma–ray in the upper and lower detector respectively. The technique used by COMPTEL to image point sources is described in Sect. 3.1.1. Further detailed descriptions of the operational principles of the COMPTEL instrument may be found in Schönfelder et al. (1984, 1993).

The "single detector" (or "burst") mode is triggered upon receipt of a signal from the CGRO-BATSE detector that a burst is in progress. In this instance, two of the lower NaI detectors (called D2-7 and D2-14) accumulate 6 high time resolution ('burst') spectra for an integration time of either 0.5 s or 1 s for the data presented here, followed by 133 'tail' spectra, each of 6 s integration time. Thereafter the burst modules return to 'background mode', integrating spectra for 100 s and awaiting the next BATSE trigger. The background mode spectra are mainly used for the background subtraction of burst and tail spectra.

The burst modules (each with a detecting area of 615 cm^2) operate in two overlapping energy regions. The low range detector (D2-14) is sensitive between 0.3 – 1.3 MeV while the high range module (D2-7) covers the energy interval 0.6 – 10 MeV (122 and 128 energy channels respectively). The spectral resolution is 9.6% at 0.5 MeV and 7.0% at 1.5 MeV. Data from both detectors exist only for GRB 910425 and GRB 910503, after which time the low energy module was switched off due to increased HV noise. Further instrumental details may be found in Winkler et al. (1986) and Schönfelder et al. (1993).

This paper focusses on the results from gamma–ray bursts which were detected in the FOV of the COMPTEL instrument in the first year of operation, up to April 16 1992. Preliminary results for some bursts have already been presented in e.g. Collmar et al. (1993), Winkler et al. (1992a, 1992b), Connors et al. (1993) and Varendorff et al. (1992).

2. Observations

BATSE detected more than 200 cosmic gamma–ray bursts between April 17 1991 and April 16 1992. The COMPTEL burst detectors (modules D2-7 and D2-14) are, in principle, 4π sensitive. In practice, however, their field of view is obstructed by a considerable amount of mass from both COMPTEL itself and the rest of the CGRO spacecraft. Bursts with a zenith angle less than 45° which have been directly localised by COMPTEL are included in this paper because the sensitivity of the instrument in the forward direction is high and relatively uniform so that the same response matrix can be used for different bursts (see Schönfelder et al. 1993). The remaining bursts were selected if they had a zenith angle less than 40° according to the original BATSE trigger messages, in order to conservatively allow for possible errors on the BATSE location.

Table 1 presents the BATSE trigger numbers, the dates and the onset times of all the gamma–ray bursts which meet the zenith angle requirement. In total there are 28 bursts, but data are not available for 6 of them, due to real–time telemetry data gaps or instrument shutdown, resulting in a total COMPTEL dataset of 22 bursts.

Table 1. Summary of Observations

COMPTEL FOV bursts		
BATSE	Burst ID	
Trigger	Date	Seconds (UT)†
109	910425	2265.75
143	910503	25452.7
249	910601	69734.55
298§	910609	2907.16
451	910627	16157.78
503	910709	41602.13
537§	910714	74777.11
678	910814	69273.03
692	910818	49485.97
829‡	910927	84412.81
856	911002	31971.8
1051	911113	49304.02
1085	911118	68258.06
1125	911127	83314.33
1154	911209	3408.02
1197	911219	79038.1
1211	911224	21944.21
1221	911225	61717.52
1297	920113	75138.77
1298	920114	62626.46
1318	920127	77217.43
1365	920207	6261.4
1469‡	920308	63223.96
1493‡	920318	54417.96
1510‡	920321	84899.96
1517‡	920324	75266.96
1550‡	920412	72123.96
1551	920413	82531.99

† Due to a CGRO clock error, 2.04 s should be added to these times to obtain uncorrected CGRO time

‡ Not detected by COMPTEL due to telemetry gaps, bit errors or instrument shutdown

§ These weak events were imaged by COMPTEL and are less than 45° off-axis, but have large (∼ 10°) errors on their positions due to the small number of imageable events

3. Analysis techniques

3.1. Double scatter mode

3.1.1. Imaging

COMPTEL is uniquely capable of imaging strong gamma–ray bursts (S(> 1 MeV)> 10^{-6}erg cm^{-2}) which occur within the FOV of the telescope. Events are sorted in a 3-D data space, defined by the co-ordinates of the scatter direction (χ, ψ) and a scatter angle $\overline{\phi}$ (see Eq. 1). A search for a burst source in this 3-D data space is then carried out using a maximum likelihood analysis which provides quantitative information on the detection significance and the source location. For each position in the COMPTEL FOV, the maximum likelihood can be calculated for either a background distribution explaining the data (the null hypothesis), or for a background distribution plus

a point source. The maximum likelihood ratio for these tests provides a measure for the likelihood that a source has been detected. This technique as applied to the COMPTEL data is fully described by de Boer et al. (1992).

The COMPTEL images for the stronger bursts are presented. The 1-, 2- and 3σ error contours are given and reflect only the statistical errors on the burst positions. Systematic errors are of the order of 0.5°. Typical 1σ contours for the strongest bursts have a radial extent of $\sim$ 0.5°, whereas for the weaker bursts, this value is in the 2° – 5° range. The maps are in galactic co-ordinates, with an $(\alpha, \delta)_{2000}$ grid superimposed.

To facilitate follow-up counterpart searches, the arcs derived from Ulysses-BATSE and where available, Ulysses-PVO and BATSE-PVO, burst arrival time differences are included in the maps. In all cases there is good agreement between the positions obtained by these two independent methods. The COMPTEL error region can thus be used to reduce the size of the sky region to be searched for counterparts at other wavelengths.

3.1.2. Spectral deconvolution

Spectral deconvolution of the telescope data is less straightforward than for single detector mode data. The procedure is simplified when the data are selected such that the COMPTEL energy response is nearly diagonal. Deconvolution in this case reduces from matrix inversion to simple scalar multiplication. The COMPTEL response is diagonalized by selecting only those events whose event-circles pass near the derived source position. This selection effectively eliminates incompletely absorbed photons. Although this procedure reduces detection efficiency, it also has the effect of significantly reducing background, as well as forcing the response to be nearly diagonal.

Monte Carlo simulations are used to compute the COMPTEL telescope response to a trial photon spectrum at the proper burst location, which is obtained from maximum likelihood fitting. The diagonal response is found to be relatively insensitive to the shape of the trial photon spectrum as long as the energy bins are significantly wider than the COMPTEL energy resolution. Identical data selections are imposed on both the simulated and measured events in order to most accurately model the response. The simulated response is then used to determine the burst photon flux from the observed count spectrum (corrected for deadtime effects) by direct scalar inversion.

Only high signal to noise bursts are analysed, thus no background subtraction is performed. When the resulting photon spectrum differs significantly from the trial photon spectrum used in simulation, a new response is generated using a new choice of trial spectrum. Parameter testing is performed by fitting a model photon spectrum folded through the simulated response to the observed count spectrum. In comparing the model spectrum with the data, maximum likelihood statistics are used instead of χ^2 due to the typically low number of observed counts. In this analysis, data are chosen using standard time – of – flight, pulse shape and energy selections, as well as the constraint that the event-circle pass within 10° of the most likely source position.

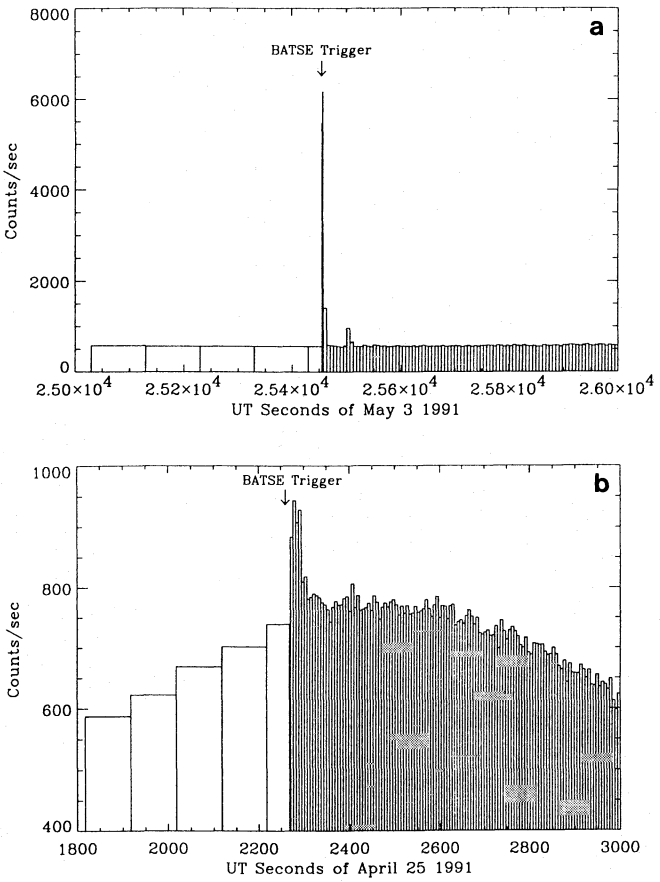

Fig. 1a and b. Two examples of raw burst time histories from the D2-14 burst module (0.3–1.3 MeV), showing different background behaviours **a** Upper panel: GRB 910503 **b** Lower panel: GRB 910425

The greatest uncertainty in the telescope spectra is the overall normalisation due to uncertain livetimes, which is of the order of 20–50%. The errors shown on the telescope spectra normalisations are simply the statistical errors from the fitting and do not incorporate this uncertainty.

3.2. Single detector mode

3.2.1. Background subtraction

Fig. 1a and b shows the time histories of two bursts on typical backgrounds. Normally, the default background used in subtraction is the spectrum of the last complete 100 s integration before the occurrence of the BATSE trigger. The default background subtraction has been applied to all the bursts in the burst mode data, with the exception of GRB 910425 and GRB 910627. All the single detector data which have been analysed have been deadtime corrected, since there are small, but non-negligible, deadtime effects in the single detectors.

For GRB 910503, the choice of spectrum to use as a background is made straightforward by the fact that the burst sits on a flat background. Thus, the default spectrum, starting at t=25330 s, may be regarded as a good approximation to the true background during the burst.

In Fig. 1a and b **b**, the time history of GRB 910425, including background, is shown. The moderate intensity of this burst combined with the steeply increasing background at the time of the burst, make the default background (starting at t=2110 s) a poor choice in this case. An improved background estimate for GRB 910425 was obtained by fitting the background region around the burst (excluding the burst itself) by a polynomial function. The fit function was interpolated to cover the time interval containing the burst and then subtracted. Separate fit functions for the low and high range detectors were required because of the energy dependence of the background count rate.

3.2.2. Spectral fitting

The spectral fitting of the data from the two burst modules involves the use of a standard forward folding technique, whereby a trial photon spectrum is convolved with the response matrix and compared with the observed spectrum in count space. A χ^2 test establishes the goodness of fit of the model. The observed photon spectrum is then constructed from the observed count spectrum, scaled by the ratio of the model photon spectrum to model count spectrum.

Single power law, broken power law and optically thin thermal bremsstrahlung (OTTB) functions are used as trial photon models, however the latter two are only used where a single power law results in an unacceptable fit. The single power law model is described by the form $\mathbf{a}\times\mathrm{E(MeV)}^{-\alpha}$, where **a** is the normalisation, or flux at 1 MeV (in photons/(cm^2 s MeV)) and α is the spectral slope .

Uncertainties in the best fit parameter values are estimated according to Lampton, Margon and Bowyer (1976), whereby the parameter space between the ${\chi^2}_{min}$ and ${\chi^2}_{min}$ + 4.61 for two parameter fits (i.e. single power law and OTTB), or ${\chi^2}_{min}$+7.78 for a four parameter fit (broken power law) determines the 90% (1.6σ) confidence interval for the set of parameters simultaneously. *Unless otherwise stated, the errors quoted for the spectral fitting results in this paper refer to the* 90% *confidence interval for the model.* In certain circumstances, single parameter of interest errors may be quoted, when the behaviour of a single parameter rather than a model is being examined. In such cases, the 90% confidence interval for the parameter of interest is determined by the extent of the parameter space between ${\chi^2}_{min}$ and ${\chi^2}_{min}$ + 2.71.

In order to ensure that there are sufficient counts in each energy bin to make the Gaussian approximation (hence χ^2 analysis) valid, the data have been rebinned. The rebinning algorithm takes a user specified number of σ (i.e. n σ) and starting at the high energy end of the spectrum, sums bins containing background subtracted counts until the number of counts in the new bin is n σ above the error on the counts in the new bin. Rebinning with n = 3 has been applied to all the spectra which are discussed in this paper. We have studied the effects of a variety of binning procedures on our fit results and have found no significant effect on the best fit results obtained.

The standard energy ranges used in spectral fitting are 0.3 – 1.3 MeV (low range, module D2-14) and 0.6 – 10 MeV (high range, module D2-7). The low energy threshold for fitting is determined by the lower limit to the current response matrix. Future improvements in the determination of the response matrix may bring the low energy threshold of the D2-14 detector closer to the 100 keV limit defined by the electronics.

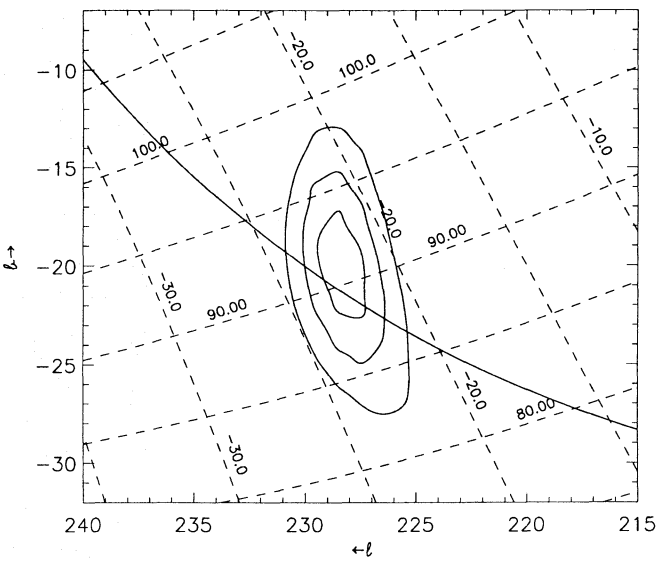

Fig. 2. COMPTEL map of GRB 910425, showing the BATSE-Ulysses triangulation arc

3.2.3. Spectral evolution

Hardness ratios are calculated, using data from the high range module only, by taking the ratio of background subtracted and deadtime corrected counts in the ranges 2 – 10 MeV and 0.6 – 2 MeV.

3.3. Time histories

Time histories may be generated from both the telescope data and from the burst modules. For the telescope, event selection windows, applied to energy deposit, time – of – flight and pulse shape, are employed to reduce the background. Once the source has been imaged, then a further event selection is made such that only events within ±10° of the most likely source position are accepted. The telescope time histories have a maximum time resolution of 100 ms, while those from the burst modules have a resolution defined by the mode of the detector, i.e. background, burst or tail mode (integration time of 100 s, 0.5 s or 1 s and 6 s respectively).

The telescope time profiles are examined by eye for evidence of anomalous emission in the form of precursors, postcursors and periodicities. This is possible only with the telescope data because events are continuously accumulated, whereas high time resolution with the burst modules is obtained only immediately *after* receipt of a BATSE trigger.

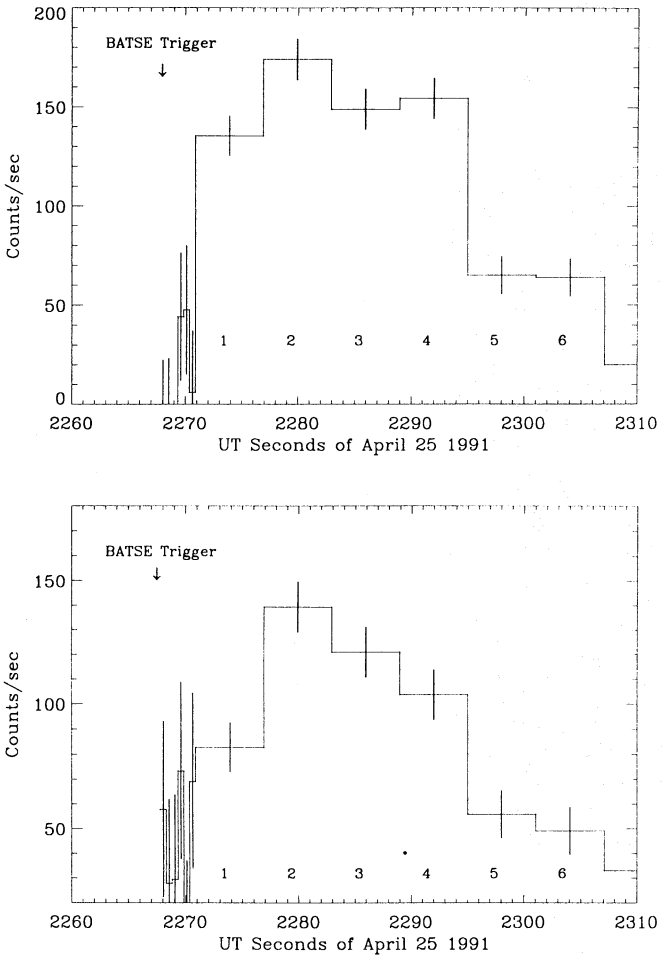

Fig. 3. Background subtracted time histories for GRB 910425 from the single detector data. Upper panel: D2-14 (0.3–1.3 MeV). Lower panel: D2-7 (0.6–10 MeV)

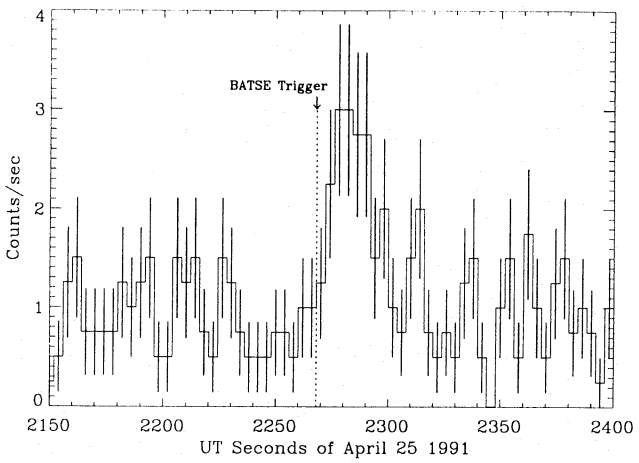

Fig. 4. Telescope time history for GRB 910425 (0.7–30 MeV) with 4 s time binning

Table 2. GRB 910425: Best fit spectral slopes from single power law model fits to the time resolved single detector spectra. Note that the errors quoted are 90% errors for the two parameter model fits

Time interval	D2-14: 0.3 – 1.3 MeV		D2-7: 0.6 – 10 MeV	
	α	χ^2/ν	α	χ^2/ν
1	2.15 ± 0.43	7/15	2.31 ± 0.60	1.3/4
2	2.05 ± 0.38	17/22	2.10 ± 0.34	7/9
3	2.50 ± 0.45	11/17	2.20 ± 0.35	10/8
4	2.62 ± 0.42	17/17	1.92 ± 0.46	7/6
5	1.79 ± 0.77	4/4	1.64 ± 1.08	2/1
6	3.02 ± 0.92	2/3	2.20 ± 1.20	1/1
Total (39 s)	2.45 ± 0.23	28/38	2.10 ± 0.23	13/15

4. Results

In this section, detailed results are presented for the brightest FOV bursts in chronological order. The remaining weak FOV bursts are dealt with in Sect. 4.8.

4.1. GRB 910425

GRB 910425 was the first burst to be detected by COMPTEL within its field of view (Fig. 2).

The main emission from the burst lasted for about 39 s (Fig. 3), with the maximum emission occurring about 10 s after the BATSE trigger. The onset of emission in both the single detectors and also in the telescope (see Fig. 4) occurred approximately 3 s after the BATSE trigger. The burst profile consisted of a single pulse with a sharp rise and a slower, smooth decay. The burst had a fluence $S(\geq 0.6\,\mathrm{MeV}) = (5.5 \pm 1.4) \times 10^{-5}$ erg cm^{-2}.

The deconvolved photon spectra obtained from the low and high range burst modules for the entire burst duration (39 s from the trigger time) are shown in Fig. 5. A single power law model sufficed to fit the time averaged data, with a best fit spectral slope of 2.45 ± 0.23 from the D2-14 detector and 2.1 ± 0.23 from the D2-7 detector (see Table 2). The telescope spectrum (Fig. 6) for the same time interval yields a value of 1.73 ± 0.38 (90% error) for α. The discrepancy ($\sim 1.7\sigma$) between the slopes from the D2 modules and the telescope may be due to inadequacies in the on-axis response matrix for this burst, which occurred 44.8° off-axis, just within the FOV. Further work is underway to reanalyse the data using a response matrix generated for a burst at the position of GRB 910425.

Individual 6 s tail spectra, as labelled in Fig. 3, were deconvolved in order to study the spectral evolution of the burst on a timescale of 6 s (Table 2). These are also adequately described by a single power law model. Within the errors, there is good agreement between the power law indices obtained from the high and low range burst modules. The exception is the fourth tail spectrum, where the low range α seems excessively soft. If the 1σ errors on α only are considered, then the high and low range α for each time interval agree to within 1.2σ, except for the 4^{th} tail spectrum, where they differ by 2.5σ.

From Fig. 7, it appears that the discrepancy in α between the two detectors for this time interval may be attributed to a possible additional soft component observed between 300 and 450 keV in

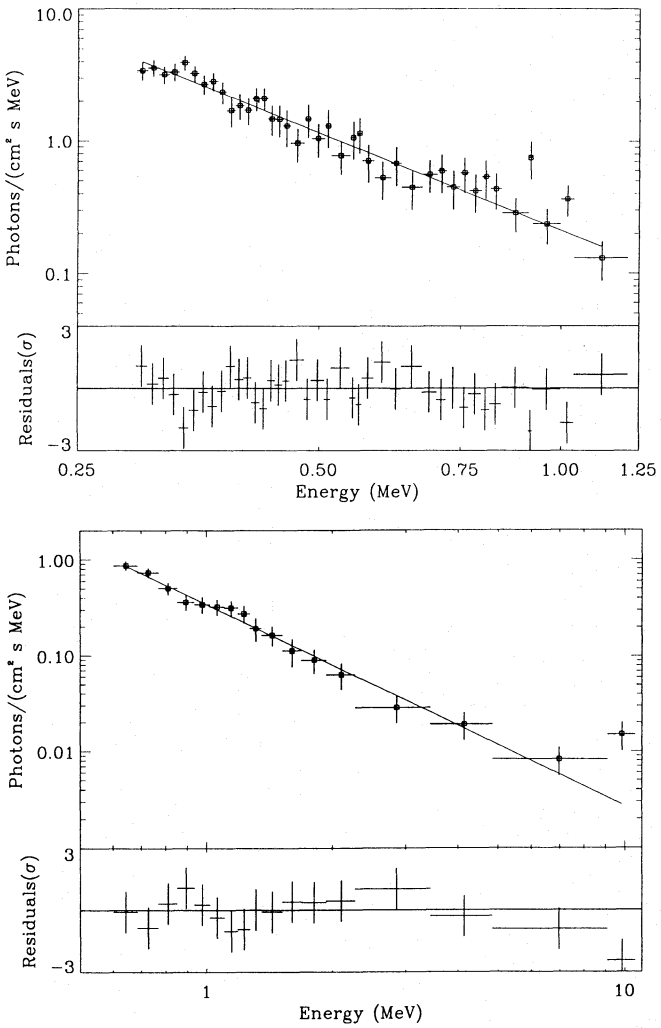

Fig. 5. GRB 910425: The upper panel shows the deconvolved spectrum for 39 s of data from D2-14 and the lower panel shows the equivalent spectrum obtained from the D2-7 detector

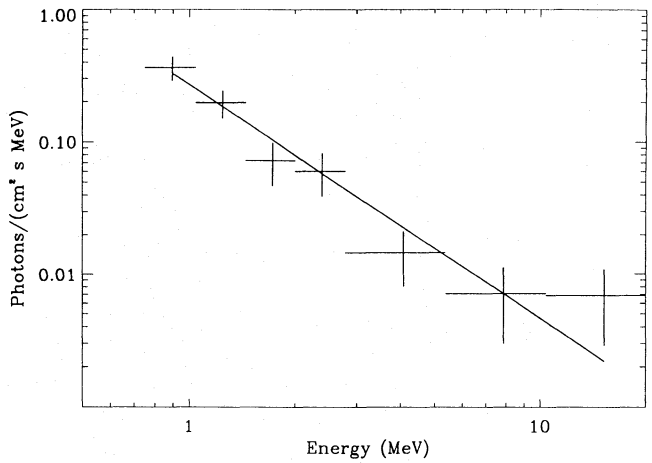

Fig. 6. Telescope spectrum for 39 s of GRB 910425, $\alpha = 1.73 \pm 0.38$

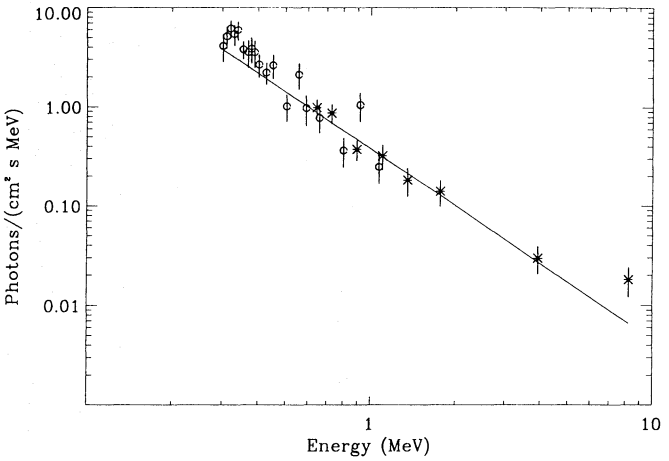

Fig. 7. The straight line represents the best high range model for the 4^{th} tail spectrum of GRB 910425, extrapolated to low range energies. The circles are the low range data points and the asterisks are the high range data points. There is good agreement in the overlap energy region, but a soft excess between 300 and 450 keV is visible in the low range detector data

the low range spectrum of the 4^{th} tail (time interval 4). This was confirmed by re-analysis of the D2-14 data in the energy interval 0.45–1.3 MeV, whereupon the α values for all time intervals in the D2-14 and D2-7 detectors were found to be in agreement to within 1σ. This feature may be interpreted as a potential 511 keV redshifted line candidate. Further study of the origin of the possible soft component (e.g. from background fluctuations) is being undertaken and will be discussed in a future publication.

No evidence of significant spectral evolution on the 6 s time scale was detected in this burst.

Spectroscopic results from BATSE have been presented for GRB 910425 in Schaefer et al. (1992), hereafter referred to as **S92**. Integrating over 39 s, BATSE obtains a single power law model with α=1.55 (minimum fit energy of 100 keV). The models with curvature do not significantly improve the fit results. This value for α is slightly harder than the COMPTEL values obtained from the independent low and high range burst modules but is in better agreement with the telescope data. The error on the BATSE slope is not known, so all the fit results may be compatible within the errors.

4.2. GRB 910503

This was the strongest burst observed by COMPTEL (S($\geq$ 0.6 MeV) = $1.5^{+0.19}_{-0.17} \times 10^{-4}$ erg cm^{-2}) during the first year of operation (Fig. 8).

At that time, 3 detectors out of 21 (D1-7, D2-1 and D2-5) were not in operation, resulting in 73% operational efficiency in the telescope mode. The time history of the telescope data (Fig. 9) demonstrates the strength of the event, since the high count rate ($\geq$ 23 Hz, normal event rate $\sim$ 6 Hz) led to a saturation of the event data buffer prior to transmission. Rapid buffer saturation prevents acceptance of further data and results in the data gaps seen in the first peak of Fig. 9 at 25457.25 s and

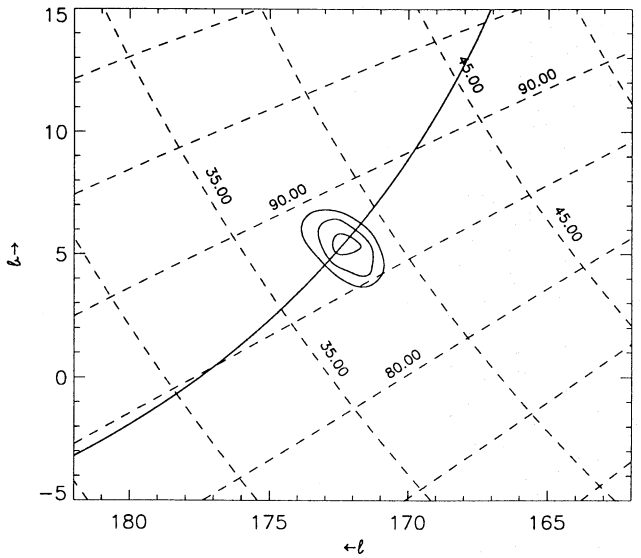

Fig. 8. COMPTEL map of GRB 910503. A preliminary triangulation arc has been published in Hurley et al. (1992a)

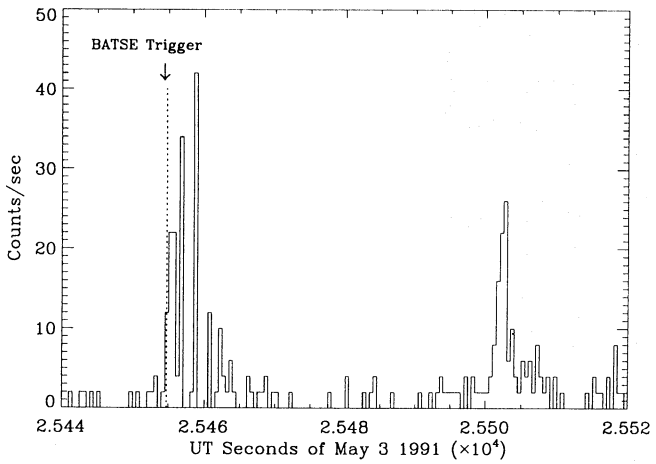

Fig. 9. Telescope time history of GRB 910503 (0.5 s binning)

25459.25 s. The sharp rise in the telescope data is also present in the deadtime corrected time history obtained from the single burst detector modules (Fig. 10).

GRB 910503 consists of two pulses (9 s and 12 s duration) separated by 36 s. The total duration is thus $\sim$ 57 s. The interpulse region shows no evidence for burst emission and is consistent with the pre-burst background level.

The hardness ratio (Fig. 11) shows that significant hard-to-soft evolution was observed during the first pulse of the burst. The poor statistics in the second pulse make it impossible to determine whether or not there was any spectral evolution.

Time integrated spectra for the first pulse (1), the second pulse (2) and the full burst duration (3), have been deconvolved and single power law models were found to produce acceptable fits. The power law indices for the single detector modules and the telescope are summarised in Table 3.

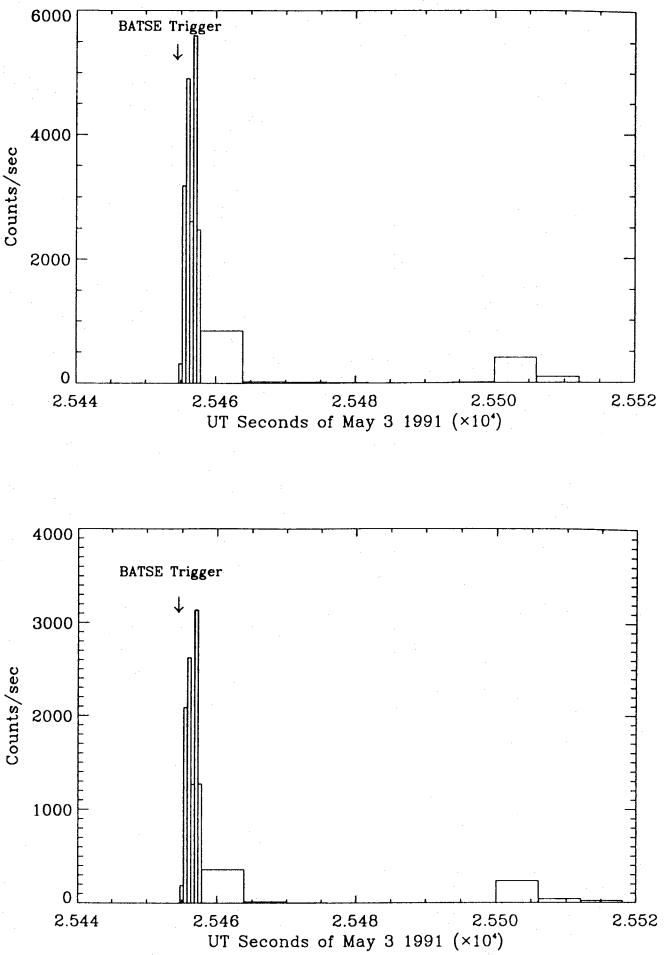

Fig. 10. Background subtracted time history from the low range burst module (0.3–1.3 MeV) (upper panel) and from the high range detector (0.6–10 MeV) (lower panel) for GRB 910503

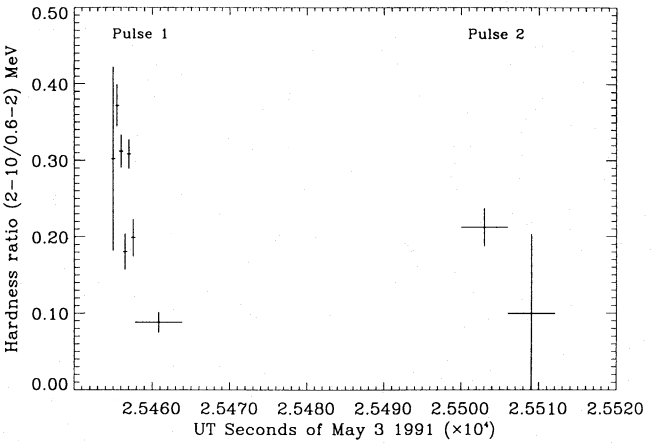

Fig. 11. Hardness ratio for GRB 910503, showing significant softening in the first pulse of the burst

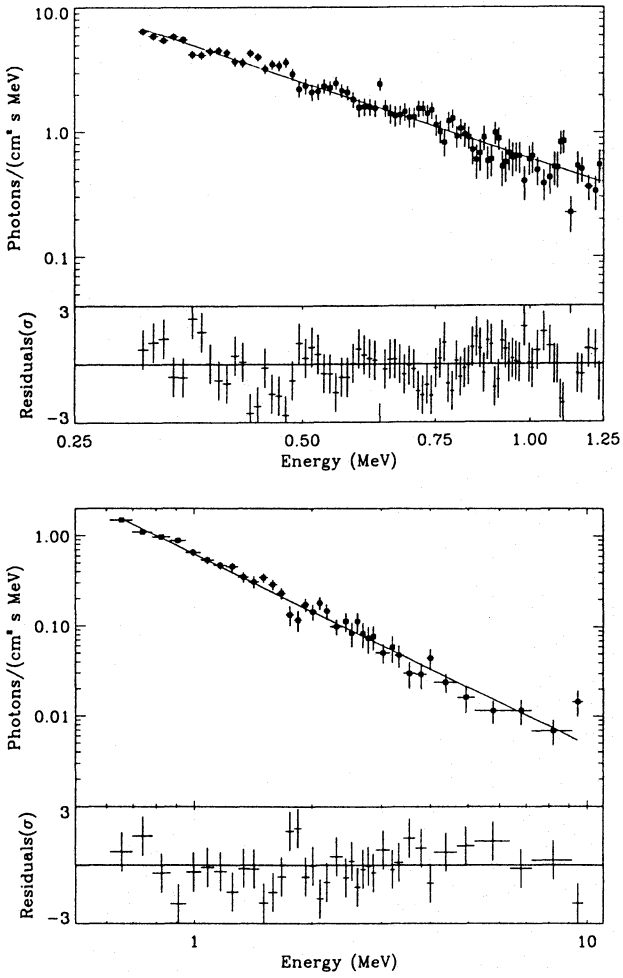

Fig. 12. GRB 910503: Deconvolved photon spectra for the full 57 s of the burst. The D2-14 and D2-7 spectra are shown in the upper and lower panels respectively

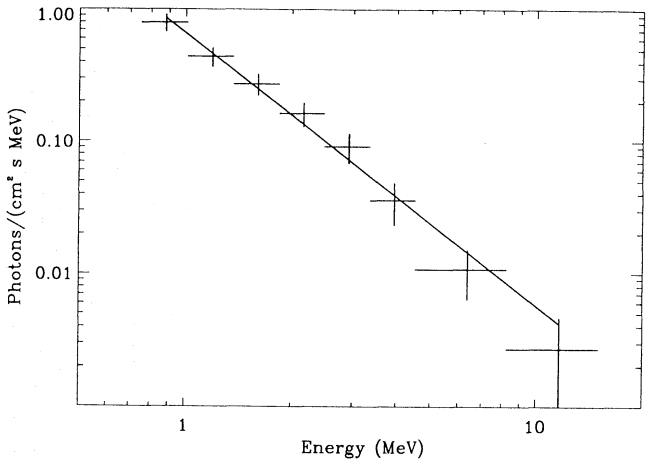

Fig. 13. GRB 910503: Deconvolved telescope spectrum for the full 57 s of the burst, $\alpha = 2.06 \pm 0.27$

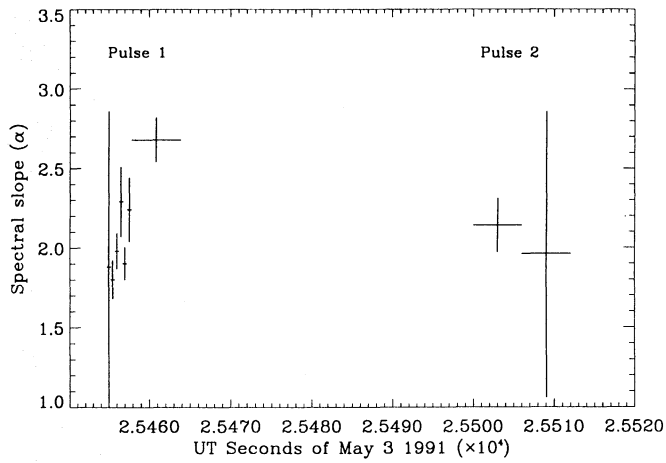

Fig. 14. Power law indices of GRB 910503 as a function of time, indicating the softening of the spectrum in the first burst pulse

Photon spectra derived for the full burst (time interval 3) from single detector and telescope data are shown in Figs. 12 and 13.

In addition, the individual spectra from the burst modules were deconvolved. All 6 burst and 3 tail spectra measured by both burst detectors during the two pulses can be fit by a single power law model except the low range spectrum obtained in the last 6 s portion of the first pulse, where a single power law is to be rejected (χ^2 = 38 with 17 degrees of freedom) and a broken power law gives acceptable fit results (α_{low} = 1.90±0.5, α_{high} = 3.50 ± 1.05, E_{break} = 1.3 ± 0.5 MeV, χ^2/ν = 16/14).

The power law indices from the individual spectra as a function of time are shown in Fig. 14 and confirm the softening of the spectrum in the first pulse observed in the hardness ratio.

To compare data from BATSE and COMPTEL for GRB 910503, the burst mode data were reanalysed to coincide as closely as possible to the time intervals used in **S92**. The results are shown in Table 4.

Out of the three time intervals shown in Table 4, a single power law is rejected by the BATSE data for the 0–15 s and 0–2 s intervals, but may not be rejected in the COMPTEL data. For the 2–3 s interval, the two instruments give consistent results, in terms of both the model and the best fit spectral slope. EGRET results for this burst (Schneid et al. 1992) are in good agreement with the COMPTEL values. For the first 3 s of the burst, EGRET sees a power law spectrum, (α = 2.13±0.08 for the first second, α = 2.24 ± 0.03 for the second through third seconds) while for the following 4 s, a single power law cannot be fit to the data. This agrees with our observation of a broken power law (E_b = 1.3 ± 0.5 MeV) for the interval 4–9 s after the BATSE trigger.

4.3. GRB 910601

This burst (Fig. 15) had a fluence of S(≥ 0.6 MeV)= $3.53^{+0.87}_{-0.63} \times 10^{-5}$ erg cm^{-2}.

The time history of this event (Fig. 16) shows that the main burst emission followed approximately 10 s after the BATSE trigger. The event lasted a total of 33 s. Visual inspection of the

Table 3. Spectral fitting results from the single detectors and the telescope for GRB 910503. Note that 90% errors on two parameter model fits are quoted

Time interval	Low range (D2-14) 0.3 – 1.3 MeV		High range (D2-7) 0.6 – 10 MeV		Telescope 0.75 – 15 MeV
	α	χ^2/ν	α	χ^2/ν	α
1	2.02 ± 0.08	116/91	2.15 ± 0.05	65/58	2.02 ± 0.37
2	2.06 ± 0.21	36/44	2.17 ± 0.18	17/18	2.04 ± 0.40
3	2.03 ± 0.09	99/81	2.12 ± 0.09	39/36	2.06 ± 0.27

Table 4. Comparison of COMPTEL and BATSE results for GRB 910503. Note that 90% errors on two parameter model fits are quoted. The minimum BATSE fit energy is 300 keV

Time Interval‡	Detector	α	χ^2/ν
0–15 s	D2-7	2.02±0.07	103/91
0–15 s	D2-14	2.15±0.06	62/52
0–14 s	BATSE	2.24	64/30
0–2 s	D2-7	1.92±0.1	102/87
0–2 s	D2-14	1.96±0.07	56/49
0–1.8 s	BATSE	2.05	61/30
2–3 s	D2-7	1.93±0.1	91/82
2–3 s	D2-14	2.0±0.09	31/44
1.8–3.2 s	BATSE	2.1	39/30

‡ Relative to BATSE trigger

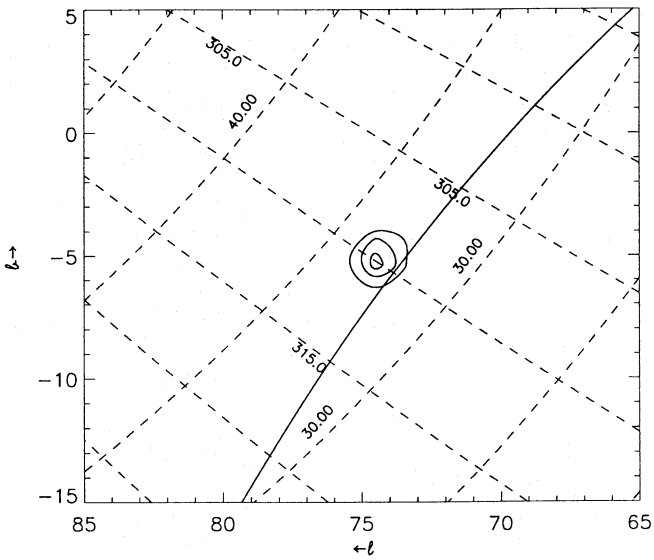

Fig. 15. COMPTEL map of GRB 910601

time history plots reveals no evidence for pre- or post-cursor emission.

The best fit photon spectrum for 33 s of high range module data from this burst (shown in Fig. 17) is a power law with $\alpha = 2.82 \pm 0.27$ ($\chi^2/\nu = 9.5/10$). Deconvolution of telescope events over the same time interval yields $\alpha = 2.79 \pm 0.38$.

The main emission detected in the burst modules occurred in the third and the fourth tail spectra. For the third tail spectrum a single power law results in a best fit value for α of 2.96±0.29, with χ^2/ν=17/8, while for the fourth tail, α = 2.84±0.22 (χ^2/ν=10/13).

No spectral evolution on the 6 s time scale was discernable from the hardness ratio or from the power law indices.

GRB 910601 was observed by all four instruments onboard CGRO. In the energy range 1–30 MeV, EGRET obtained a spectral index of 3.67±0.2 (Kwok et al. 1993), which is softer than the slopes observed by the COMPTEL burst detector and telescope. We see some evidence for a spectral turnover at 4 MeV in the telescope data since no events within ±10° of the source position are seen in the telescope above 4 MeV. There is also a hint of such a turnover in the EGRET spectrum (Kwok et al. 1993) for this burst.

OSSE has so far only published count rate spectra for this burst, with no spectral results (see Share et al. 1992).

BATSE sees significant curvature in the spectrum of this burst (described in **S92**), in particular a broken power law model which has a break energy of 0.69 MeV. This does not conflict with our observation of a single power law since the COMPTEL fit range starts just below the energy at which BATSE observes the break in slope. The BATSE slope above the break energy is 3.43, which is closer to EGRET than COMPTEL, but without error bars it is difficult to draw conclusions. The BATSE data cannot distinguish between the two models with curvature on the basis of χ^2 statistics i.e. a thermal bremsstrahlung model (kT = 0.65 MeV) is an equally good representation of the input photon spectrum. A thermal bremsstrahlung model fit to the COMPTEL burst detector data, gives a value of $kT = 0.66 \pm 0.14$ MeV, which agrees with the temperatures obtained by both EGRET (kT = 0.676 MeV) and BATSE for this model.

It is possible that the power law slope measured by COMPTEL in the burst detector is being influenced by the data point below the BATSE break energy. If this point is eliminated from the spectral fit, the best fit power law index becomes 2.97±0.36, in better agreement with the results of the other two instruments for the single power law model.

Thus, although COMPTEL cannot reject a single power law fit to these data, by combining results from other CGRO instru-

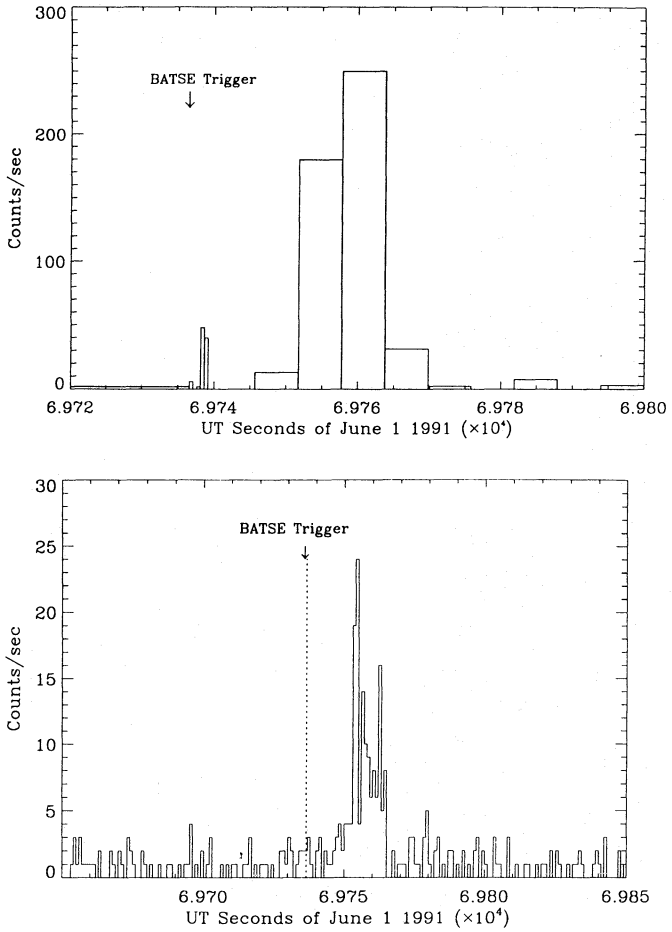

Fig. 16. GRB 910601: Upper panel: background subtracted single detector time history (0.6–10 MeV). Lower panel: telescope time history (0.75–30 MeV) with 1 s binning

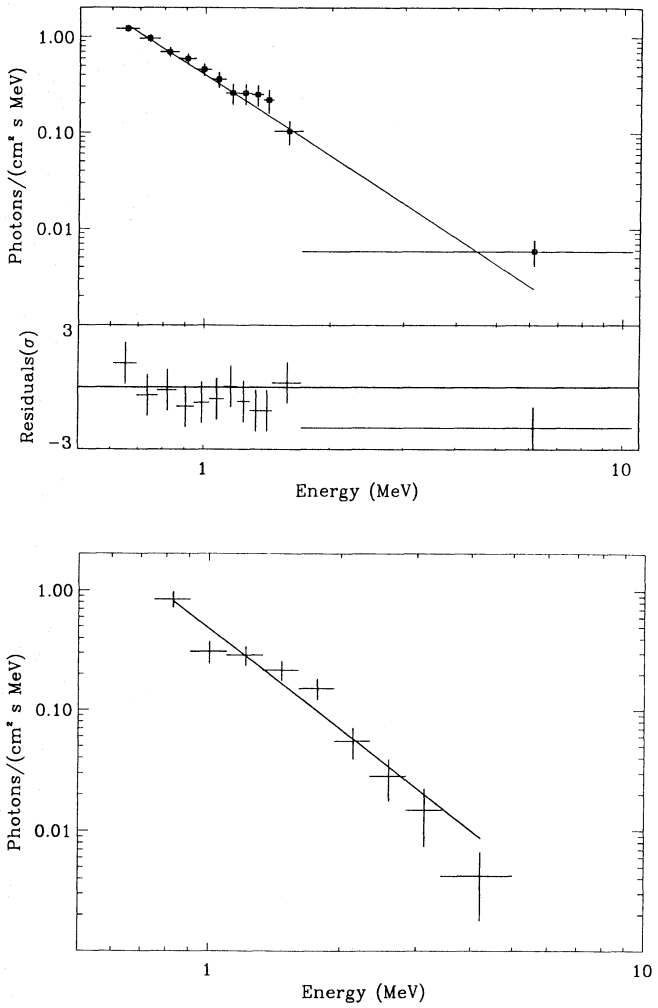

Fig. 17. Upper panel: deconvolved single detector photon spectrum for 33 s of data from GRB 910601. Lower panel: deconvolved telescope spectrum for the same time interval

ments, it becomes more likely that a model with curvature is the most appropriate for this burst.

4.4. GRB 910627

Fig. 18 shows the COMPTEL image of this rather weak burst ($S(\geq 0.6$ MeV$)= (2.6^{+14.4}_{-2.1}) \times 10^{-6}$erg cm^{-2}. The large uncertainty in the fluence arises from the poorly constrained fit parameters.

The spectral slope from the single detector for the first 2 s of the burst is $\alpha = 1.6^{+1.12}_{-0.8}$, while the telescope deconvolution yields $\alpha = 1.12 \pm 0.68$. The telescope time history and spectrum for this burst are shown in Figs. 19 and 20 respectively.

There is a hint in the telescope data, at the 2σ level, for a cut-off above 4 MeV in the spectrum of this burst.

4.5. GRB 910709

A rather unremarkable burst (Fig. 21), whose main emission was coincident with the BATSE trigger and which lasted for ~ 0.5 s.

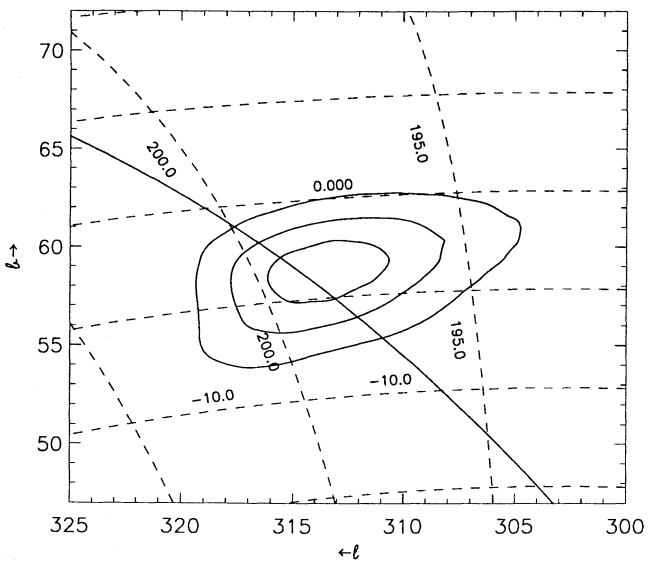

Fig. 18. COMPTEL image of GRB 910627. A preliminary triangulation arc has been published in Cline et al. 1993

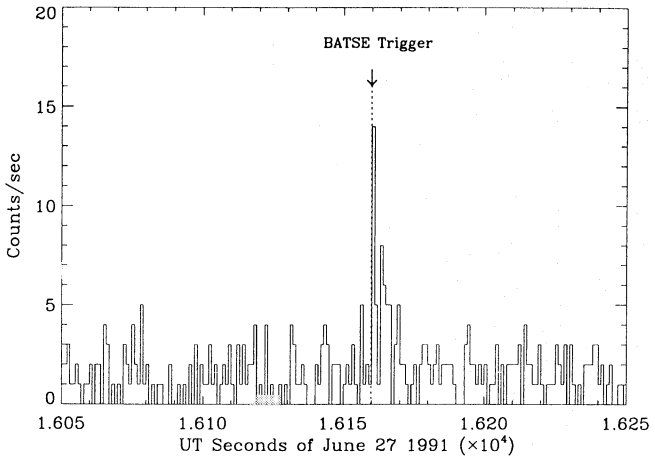

Fig. 19. Telescope time history for GRB 910627 with 1 s binning

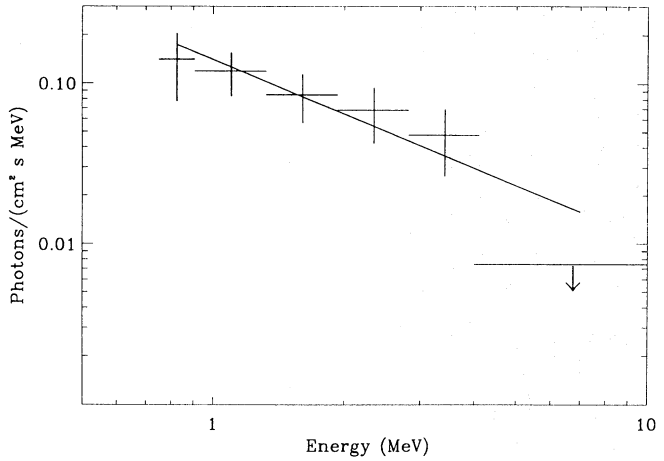

Fig. 20. Telescope spectrum for GRB 910627, $\alpha = 1.12 \pm 0.68$. The last data point is a 1σ upper limit

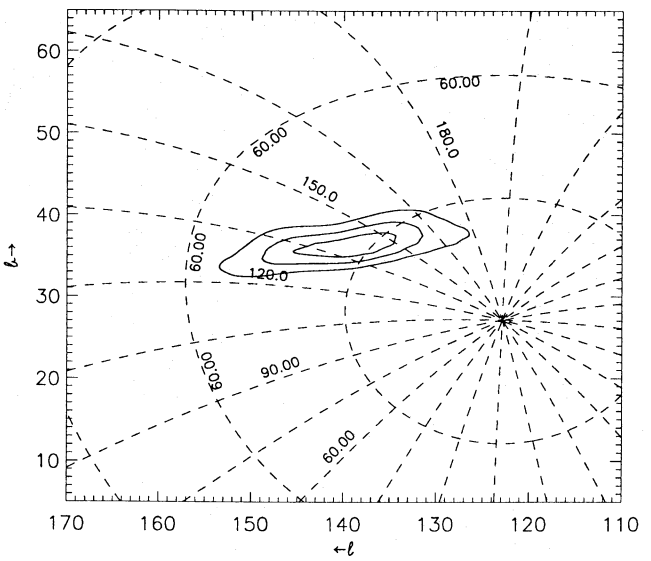

Fig. 21. COMPTEL map of GRB 910709. No triangulation arc is available for this GRB

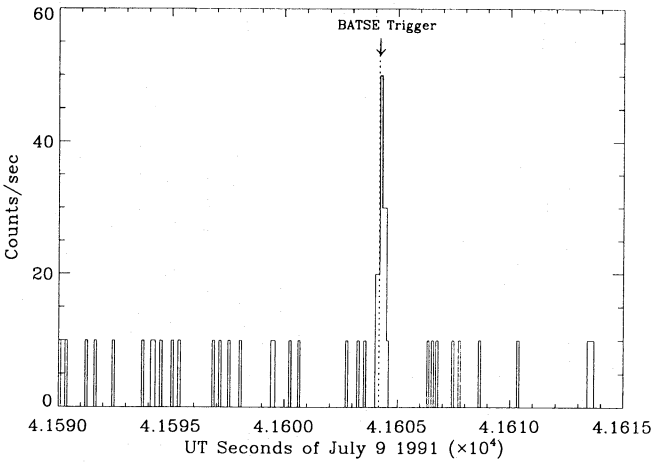

Fig. 22. Telescope time history for GRB 910709 with 100 ms binning

The telescope time history for this event (Fig. 22) shows the burst lasted for 400 ms, apparently starting 100 ms before the BATSE trigger. A visual search of the data 100 s before and after the trigger reveals no significant excesses apart from the burst itself.

The best fit photon spectrum (Fig. 23) from the burst detector yields a value of 2.0 ± 0.42 for α. Spectral deconvolution from telescope events gives a best fit value for α of 2.54 ± 1.14. The fluence has been determined to be S($\geq$ 0.6 MeV)= $(2.84 \pm 1.87) \times 10^{-6}$erg cm^{-2}.

BATSE (**S92**) obtains a broken power law model for this burst, with a break energy of 0.51 MeV and a spectral slope above the break of 1.79. This is consistent with the COMPTEL result, given that the break energy is outside the COMPTEL energy range. Apparently there is significant softening in this burst because BATSE sees signal for 3 s, whereas COMPTEL sees the event for only $\sim$ 0.5 s.

4.6. GRB 910814

This is the second most intense burst which COMPTEL observed in its first year (Fig. 24), with a fluence S($\geq$ 0.6 MeV)= $(1.3 \pm 0.13) \times 10^{-4}$erg cm^{-2}.

The burst emission above 0.6 MeV lasted about 30 s, with a typical single pulse burst profile i.e. a sharp rise followed by a slow, smooth decay (Fig. 25).

A single power law model is **not** an acceptable fit over the 33 s of the entire burst event, yielding a χ^2/ν value of 134/38. The best fit to the single detector data was obtained using a model with significant curvature i.e. a broken power law (see Fig. 26) or an OTTB. Neither model is rejectable on the basis of χ^2 statistics. The spectral break has also been observed by BATSE (**S92**) and SIGMA (Pelaez et al. 1993). The intervals marked 1, 2 and 3 in Fig. 25 represent 1 s time bins, while 4, 5, 6 and 7 are each 6 s in duration. These intervals have been used in the time-resolved spectral fitting of the burst mode spectra to

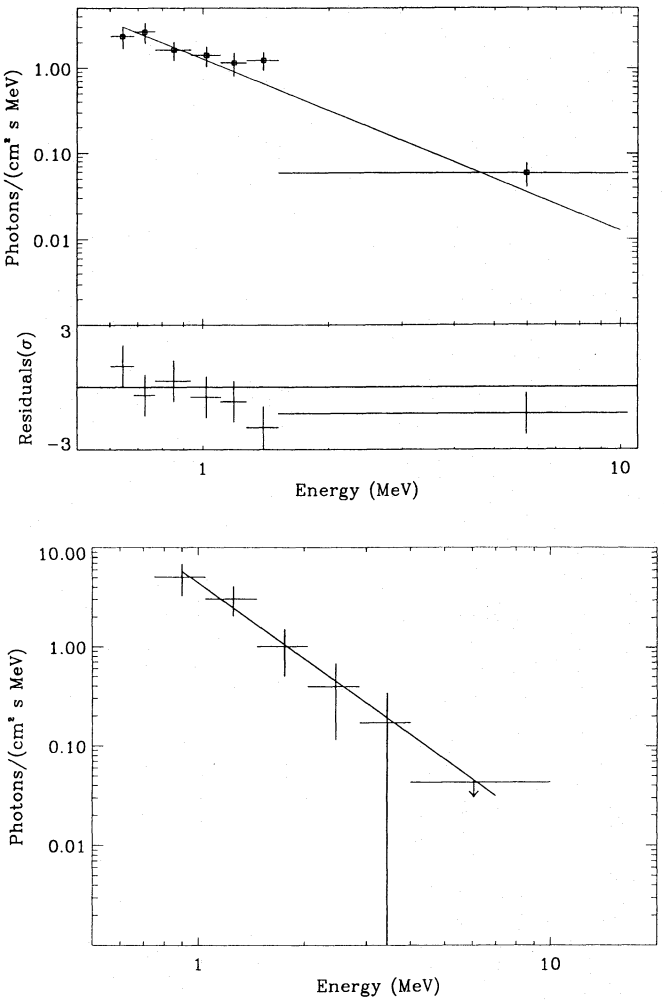

Fig. 23. Upper panel: deconvolved photon spectrum for 0.5 s of GRB 910709 from the single detector (0.6–10 MeV) (upper panel) and from the telescope (0.75–10 MeV) (lower panel)

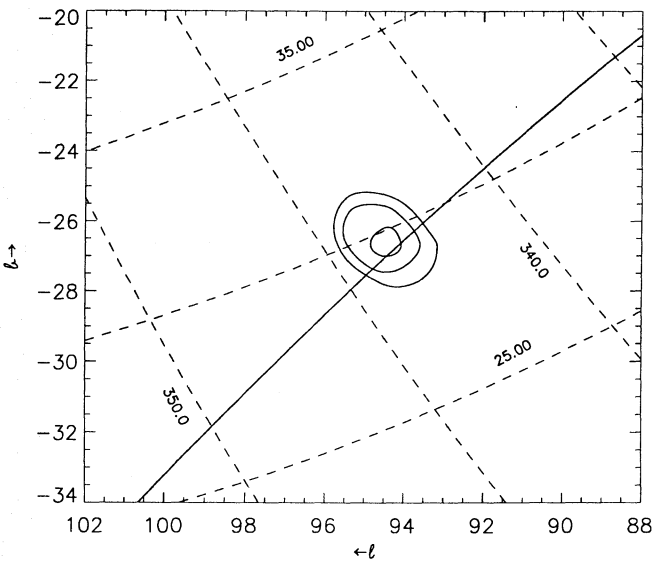

Fig. 24. COMPTEL map for GRB 910814. A preliminary Ulysses–BATSE triangulation arc has been published in Cline et al., 1992

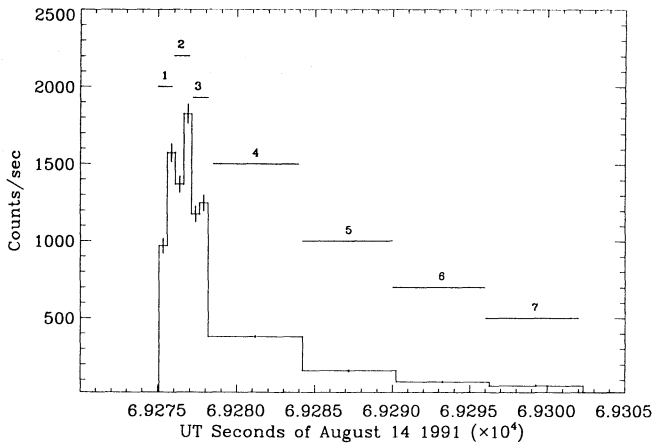

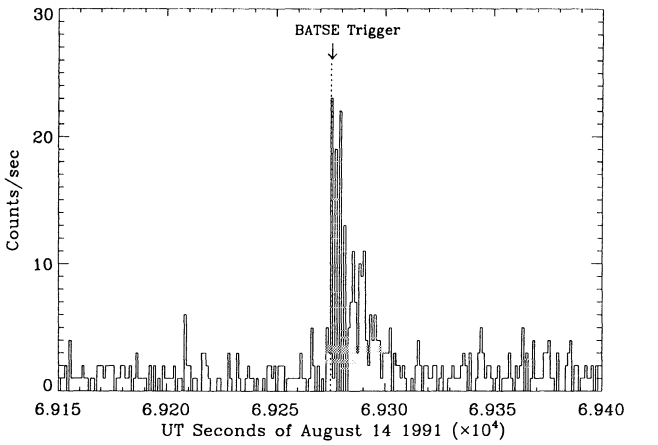

Fig. 25. Background subtracted time history (upper panel) (0.6–10 MeV) and telescope time history with 1 s binning (lower panel) for GRB 910814

investigate the spectral evolution in this burst. The results of the spectral fitting from all three models for all time intervals are presented in Table 5.

The telescope spectrum for the full burst is shown in Fig. 27 along with the best power law model. A broken power law model, with a break energy of 1.25 ± 0.3 may also be used to fit the data, however it is not possible to distinguish between these models in the telescope data since there is no measure of the goodness of fit when using maximum likelihood statistics.

The spectral curvature, requiring a broken power law or thermal bremsstrahlung model, is only significant during the first 9 s of the burst (intervals 1 to 4) after which time a single power law model is a good fit. Broken power law fit parameters after interval 5 are not shown in Table 5 since the fits could not be constrained. Fig. 28 shows the deconvolved photon spectrum for the last 18 s of the burst (intervals 5 to 7) using a single power law photon model. The best fit value for α in this case is 2.07 ± 0.18.

Table 5. Time resolved spectral deconvolution results from both the burst module and the telescope for GRB 910814. Note that 90% errors on two parameter model fits are quoted, except for the broken power law model, where the errors are 90% on four parameter model fits

Time interval	Power law		OTTB		Broken power law			
	α	χ^2/ν	kT (MeV)	χ^2/ν	α_{low}	α_{high}	E_b (MeV)	χ^2/ν
1	2.01 ± 0.11	77/28	1.97 ± 0.30	24/28	$1.41^{+0.39}_{-0.81}$	≥ 2.23	$2.08^{+2.22}_{-0.88}$	25/26
2	2.02 ± 0.10	68/33	1.98 ± 0.26	23/33	$1.58^{+0.32}_{-0.72}$	$3.61^{+2.39}_{-1.41}$	$2.74^{+1.06}_{-1.54}$	25/31
3	2.05 ± 0.11	52/26	1.86 ± 0.30	18/26	$1.5^{+0.44}_{-1.26}$	$3.04^{+2.16}_{-0.74}$	$1.91^{+1.25}_{-0.87}$	19/24
4	2.18 ± 0.10	65/24	1.44 ± 0.19	27/24	$0.6^{+1.4}_{-3.8}$	$2.62^{+0.8}_{-0.37}$	$0.97^{+0.79}_{-0.22}$	21/22
5	2.10 ± 0.21	16/13	1.70 ± 0.46	12/13				
6	2.15 ± 0.36	9/8	1.40 ± 0.64	10/8				
7	1.84 ± 0.46	3/4	2.50 ± 2.10	5/4				
Total (33 s)	2.06 ± 0.07	134/38	1.73 ± 0.15	40/38	$1.71^{+0.2}_{-0.75}$	$3.13^{+1.2}_{-0.81}$	$2.34^{+0.62}_{-1.3}$	43/36
Telescope (33 s)	2.27 ± 0.26				0.87 ± 1.3	2.62 ± 0.46	1.25 ± 0.3	

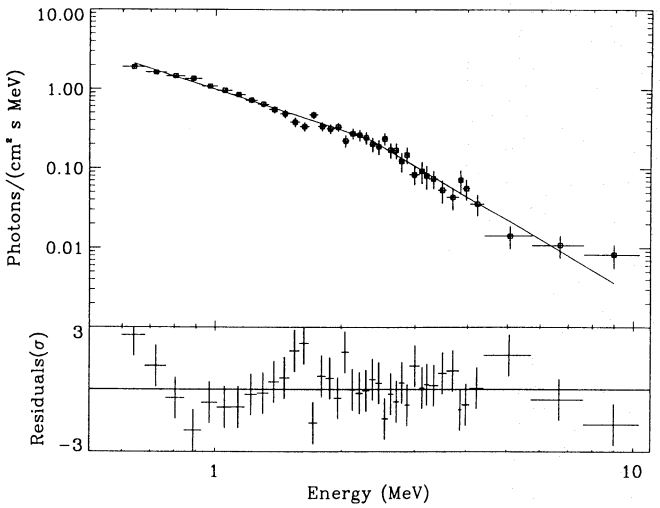

Fig. 26. Deconvolved photon spectrum for 33 s of GRB 910814 from the high range burst detector

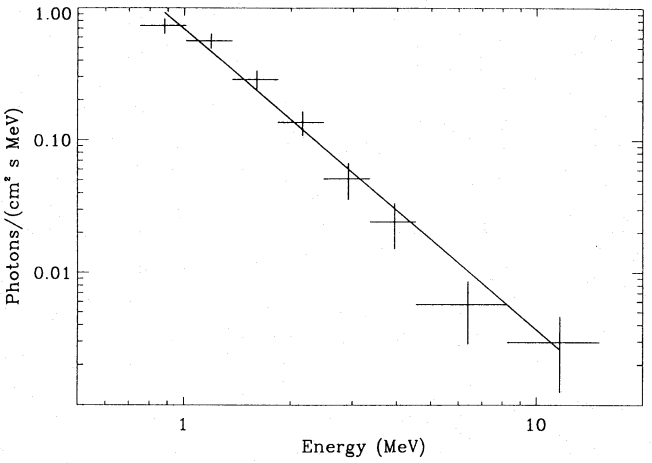

Fig. 27. Deconvolved photon spectrum for 33 s of GRB 910814 from the telescope

From Table 5 it appears that E_b is constant within the errors over the first 9 s of the burst, however, it must be borne in mind that these are 90% (1.6σ) errors for a 4-parameter model. A least squares fit to E_b versus time (shown in Fig. 29) , using one parameter of interest, 1σ errors, gives a slope of -0.254 ± 0.09. This is a 2.8σ deviation from a line of zero slope, demonstrating that there is a significant change in spectral shape, manifested as a change in E_b, during this burst.

To further test this behaviour, the burst was divided into two time intervals, $0 < t \leq 3$ s and $3 < t \leq 27$ s. For the 3 s interval the best fit value for E_b is 2.4 ± 0.31 (one parameter of interest, 1σ error), while for the second time interval the best value for E_b is 0.87 ± 0.14 (one parameter of interest, 1σ error), clearly demonstrating that a significant change in the break energy is present in the spectrum of this burst.

The time resolved spectral analysis of this GRB leads to the possibility that the break energy decreases in the course of the burst, such that after the first 9 s, it has shifted to below the energy range of the instrument. This trend may be seen in

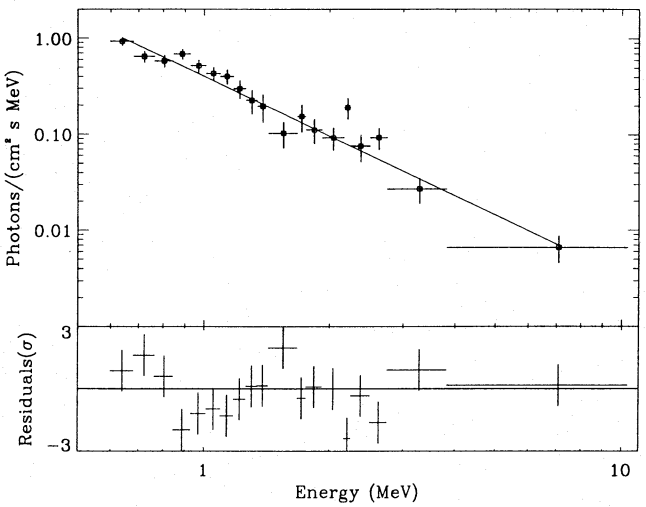

Fig. 28. Single power law model for the last 18 s of GRB 910814

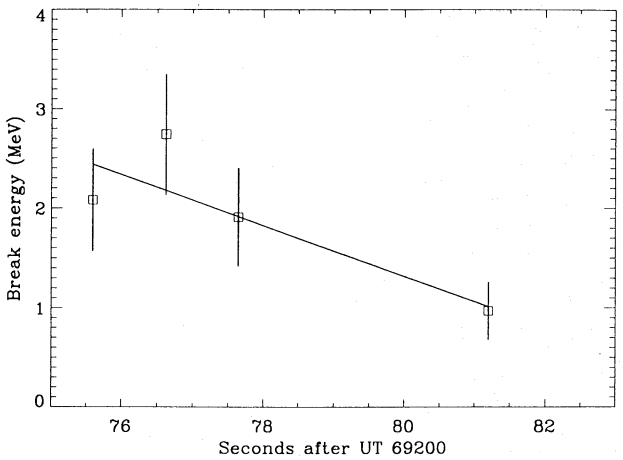

Fig. 29. Break energy of GRB 910814 as a function of time, with the best fit straight line to the COMPTEL data points. The errors on E_b are 1σ, one parameter of interest errors, derived from the broken power law model. The slope of the line is -0.254 ± 0.09

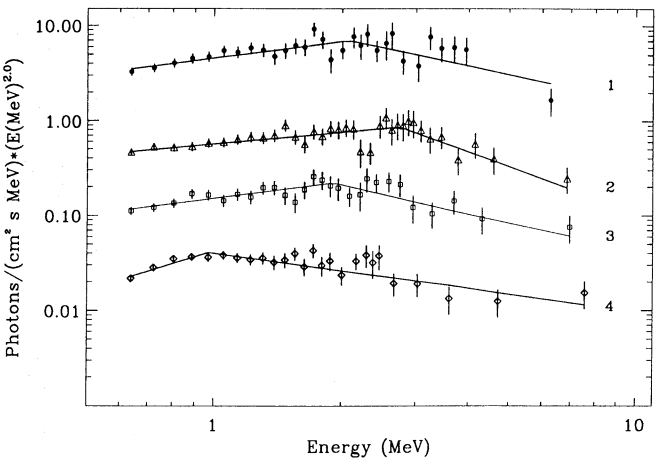

Fig. 30. Variation in break energy during the burst GRB 910814. The labelling on each spectrum corresponds to the time intervals shown in the time history plot (Fig. 25). The normalisations have been scaled so all the spectra may be shown in a single figure

Fig. 30, where the photon spectra for intervals 1–4 are plotted as $E^2 \times$Flux to indicate deviations from an E^{-2} power law.

The EGRET data (Kwok et al. 1993) from this burst support the hypothesis of a time dependent spectral break, since for the first 7 s of the burst, a single power law fits their data only if the first few points (~2 MeV) are not included in the fit. In subsequent time intervals, a single power law fits the data well over the whole energy range. The absence of error bars for the BATSE data (see **S92**) make it difficult to conclude whether or not BATSE also observes the effect. However, the combined COMPTEL and EGRET results provide clear evidence for a time dependent spectral break at MeV energies in this gamma–ray burst.

A meteor patrol plate made a serendipitous simultaneous exposure of the source region (Greiner et al. 1993). No counterpart down to $m_b = 4.5$ (for a 1 s flash) was detected. This puts a limit on the simultaneous fluence ratio of $L_\gamma/L_{opt} \geq 1300$, where L_γ was estimated in the energy range 0.6–10 MeV, over the 33 s duration of the burst.

4.7. GRB 911118

This burst (Fig. 31) had a fluence of 6.6×10^{-6} erg cm^{-2}. The time history of the event (Fig. 32) shows that the main emission followed immediately after the BATSE trigger and lasted for 9 seconds.

The best fit photon spectra for 9 seconds of data from this burst (Fig. 33), yield $\alpha = 2.64^{+.56}_{-.38}$ ($\chi^2/\nu = 7/6$) for the burst mode spectrum and $\alpha = 2.08 \pm 0.68$ for the telescope data.

The burst is just bright enough to allow limited time resolved spectroscopy (Table 6), however, due to the limited statistics, no definite conclusions as to the nature of the spectral evolution (if any) may be made.

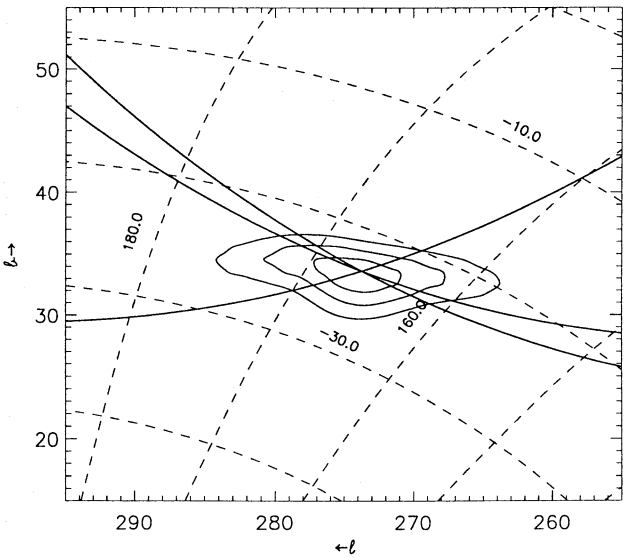

Fig. 31. COMPTEL map of GRB 911118, showing the intersection of the timing arcs from Ulysses-BATSE, Ulysses-PVO and BATSE-PVO inside the 1σ COMPTEL error contour. A preliminary triangulation arc has been published in Cline et al. 1993

4.8. The weakest bursts

The remaining bursts which occurred within the FOV of COMPTEL were too faint to be analysed in detail. 5σ upper limits on the burst fluences have been calculated and are given in Table 7.

These estimates are made by, first of all, calculating the 5σ error on the source plus background counts in the energy range 0.6–10 MeV. This is then added to the total number of background subtracted counts in the burst. The fluence upper limit is then given by:

$$S = \frac{5\sigma_{counts} \times E_{av}}{\epsilon \times A}$$

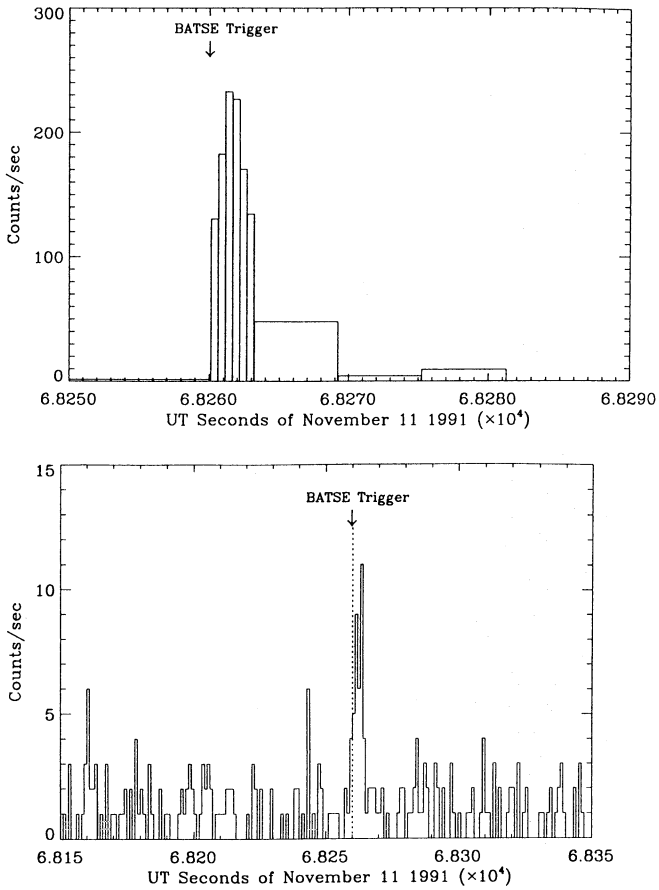

Fig. 32. Upper panel: background subtracted time history from the burst module for GRB 911118. Lower panel: telescope time history for GRB 911118 with 1 s binning

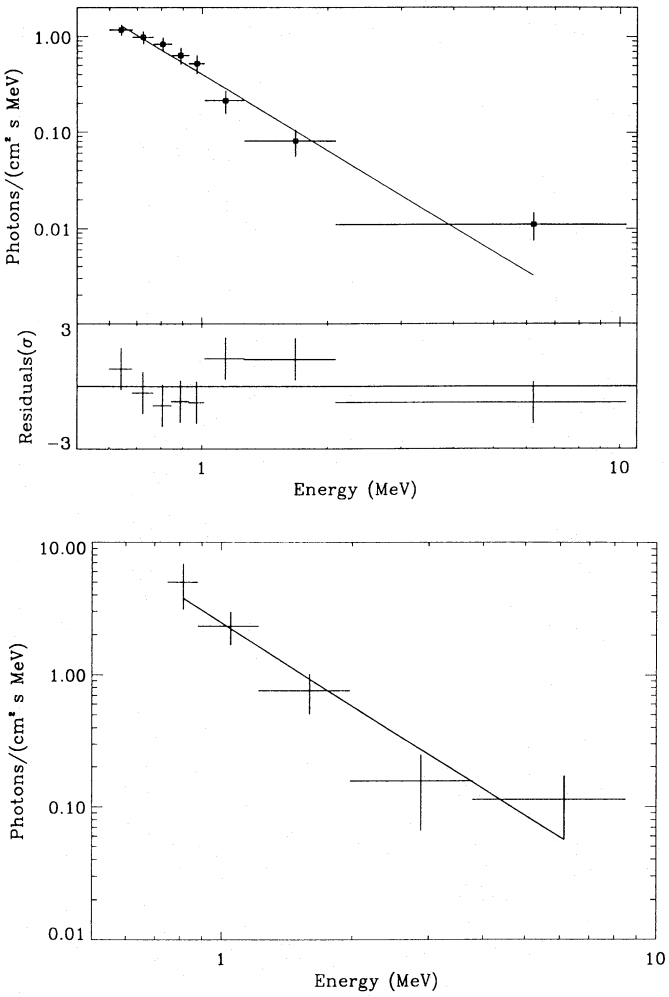

Fig. 33. Deconvolved photon spectra for GRB 911118. Upper panel shows the single detector spectrum for the full 9 s of the burst, while the lower panel shows the telescope spectrum for the same time interval

Table 6. Time resolved spectral deconvolution results for GRB 911118. The 90% errors are for the two parameter model

Time interval[a]	α	χ^2/ν
0.5–1.5	$2.4^{+0.6}_{-0.4}$	3/5
1.5–3.5	$3.0^{+0.75}_{-0.5}$	2/4

[a] Specified as seconds after the BATSE trigger.

E_{av} is the average energy, calculated by assuming a spectral index $\alpha = 2$ between 0.6 and 10 MeV, ϵ is the mean detector efficiency and A is the detector area. Since these bursts are so weak that it is not possible to make correct estimates of their duration, we assume that each burst lasts as long as the burst mode, which for these data is either 3 s or 6 s.

5. Discussion

5.1. Locations

The maximum likelihood COMPTEL positions for all the imaged gamma–ray bursts are summarised in Table 8. The appropriate error box for counterpart searches of a GRB may be determined from the maps by the intersection of the triangulation arc(s) with the COMPTEL error region.

5.2. Continuum emission

The majority of bright GRBs observed by COMPTEL had single power law spectra, with $1.6 \leq \alpha \leq 2.82$. Only one out of seven showed definite curvature, unlike the BATSE sample (see **S92**) in which roughly a quarter of bursts exhibited curvature. These are not incompatible statistics, since some of the breaks observed by BATSE are below the COMPTEL energy range (e.g. GRB 910601 and GRB 910709).

Barat (1993) has reported that for the most intense events observed between 0.1 and 9.3 MeV by the Apex experiment onboard the Phobos missions (July-August 1988 and July 1988-March 1989), a single power law shape is not an acceptable fit to the data. In fact a broken power law is the only model with curvature which adequately fits these bursts. **S92** does draw a distinction between bursts in the BATSE sample which show curvature and whose photon spectra may be described by any

Table 7. 5σ upper limits on fluence for weak FOV bursts

Burst ID	S($\geq$ 0.6 MeV) $\times 10^{-6}$erg cm^{-2}
GRB 910609[a]	3.6
GRB 910714[a]	3.3
GRB 910818[a]	2.3
GRB 911002[a]	2.8
GRB 911113[a]	4.4
GRB 911127[a]	3.3
GRB 911209[b]	0.2
GRB 911219[b]	2.1
GRB 911224[b]	3.8
GRB 911225[b]	2.3
GRB 920113[b]	5.9
GRB 920114[b]	4.5
GRB 920127[b]	1.3
GRB 920207[b]	4.2
GRB 920413[b]	7.5

[a] Assumed duration of burst is 3 s
[b] Assumed duration of burst is 6 s

Table 8. Maximum likelihood COMPTEL locations for all imaged gamma–ray bursts

Burst ID	l	b	α_{2000}	δ_{2000}
GRB 910425	228.48	-19.64	91.39	-22.21
GRB 910503	172.50	5.31	87.23	38.09
GRB 910601	74.49	- 5.35	310.14	33.05
GRB 910627	315.02	58.44	199.17	- 3.84
GRB 910709	138.49	36.52	142.19	73.82
GRB 910814	94.35	-26.72	343.44	29.54
GRB 911118	274.49	33.57	167.20	-23.57

model with curvature and those for which a broken power law is the only model which fits. As examples of the latter class, **S92** cites GRB 910503 and GRB 910814. We have examined both these bursts in detail and find definite curvature in GRB 910814, which is well fit by both a broken power law model and an OTTB. However, we find no evidence to confirm the BATSE assertion of a break in the spectrum of GRB 910503, except in one time interval (last 6 s spectrum of the first pulse) which we are unable to compare directly with the BATSE result, due to different instrumental integration times. Our observations of the continuum behaviour of this GRB agree with the EGRET results. The other time intervals where comparisons have been made for GRB 910503 (e.g. Table 3) demonstrate the agreement between both the burst modules of COMPTEL and the main instrument, for a single power law model. A significant spectral break at $\sim$ 1 MeV during the time intervals in Table 4 would definitely have been seen by COMPTEL, since both burst modules, covering 0.3–10 MeV, were operational at the time.

The observation of spectral breaks in GRBs at $\sim$ 1 MeV is usually interpreted as arising from $\gamma\gamma \rightarrow e^+e^-$ interactions in an isotropic photon distribution (e.g. Schmidt 1978). Under this assumption, Schmidt showed that the GRB distribution must be galactic since no spectral breaks had at that time been observed. The BATSE detection (Meegan et al. 1992) of an isotropic distribution of GRBs, which may imply a non-galactic origin, coupled with the observations of MeV spectral breaks, forces reconsideration of pair production processes in the light of radiation anisotropy. Baring (1993) has obtained a relationship between photon beaming angle, source distance and spectral break energy, for pair production attenuation of GRB spectra, concluding that sources which exhibit spectral breaks are either not cosmological or that their turnovers are caused by processes other than pair production. If the former is true, then ultimately we would expect a distinct spatial distribution of GRBs exhibiting spectral breaks.

The observations of spectral breaks in bright gamma–ray bursts by the BATSE, COMPTEL and EGRET instruments on board CGRO and by the Apex experiment on Phobos (Barat 1993) provoke new lines of enquiry in gamma–ray burst research. For example, it is still not clear whether spectral breaks are observed only in intense bursts because of the poor statistics of weak bursts, or whether they genuinely occur in the strongest (and therefore nearest) bursts. Mitrofanov et al. (1992) have observed a possible correlation between hardness and intensity in the Apex data. The bursts which exhibited this correlation had V/V_{max} values between 0 and 0.3. This result may turn out to be connected with the apparent correlation between the presence of a spectral break and the burst intensity. Data from many more intense MeV gamma–ray bursts are required to resolve this aspect of the spectral behaviour in these puzzling sources.

5.3. Spectral evolution

The spectral evolution in GRBs is an unresolved issue, with many conflicting reports as to its nature. Previous study of spectral evolution in gamma–ray bursts by Norris et al. (1986) concluded that the bursts observed by the GRS experiment onboard SMM showed strong evidence for hard to soft evolution in pulses on timescales of $\sim$ 1 s. The authors even point out that no example of the reverse trend (i.e. soft to hard) was found in any of the bursts in their sample. Golenetskii et al. (1983) observed an apparent correlation of hardness with burst luminosity, while Hurley (1992b and references therein) observed random variations in the hardness during a burst, apparently uncorrelated with any temporal features. In the same data, there were even cases of all three types of spectral behaviour in a single burst event. Mitrofanov et al. (1992) examining data from the Apex experiment, found a correlation between hardness and luminosity on 1 s time scales, but found no firm evidence for such a correlation on shorter time scales. Several methodological difficulties associated with hardness–intensity correlations have recently been outlined in Schaefer (1993).

In the SMM sample, 70% of bursts exhibited hard to soft evolution on time scales of $\sim$ 1 s. The remaining 30% were not observed to undergo hard to soft evolution on the 1 s time scale, but were on the 128 ms time scale. Worse still, two of these rapidly varying bursts appeared to exhibit a hardness intensity

correlation in the longer integration time data, which turned out to be hard to soft evolution in the 128 ms data. The bursts which showed significant emission at the 0.5 s time resolution in the COMPTEL data were GRB 910503 and GRB 910814. The former showed significant hard to soft evolution while the latter did not. Thus, it is not possible at this stage to confirm the SMM results, since we have only two bursts suitable for comparison with the SMM dataset.

The remaining bright GRBs which were analysed using burst module data displayed no evidence of spectral evolution, due either to poor count statistics or insufficient temporal resolution. Higher time resolution data are obtained from the telescope time histories and work is currently underway to examine these data for further evidence of spectral evolution.

5.4. Time dependence of E_b in GRB 910814

The energy of the spectral turnover in GRB 910814 was found to be time dependent. The SIGNE experiments on Venera 11 and 12 revealed that some events exhibit spectral turnovers at burst onset, at energies as high as 400 keV, which migrate to lower energies on time scales from tens of milliseconds to a few seconds (Vedrenne 1981 and Cline 1984). Hurley (1992b) observed time dependent turnovers between 50 and 70 keV in many spectra observed by SIGNE onboard Venera 13 and 14. The observation of a time dependent turnover in the spectrum of GRB 910814, from above 2 MeV to below 1 MeV, is the first report of this effect at such high energies.

6. Conclusions

We have found, for the majority of GRBs in our sample, that a power law, with α between 1.6 and 2.8, provides the best fit to the deconvolved photon spectrum in the energy range 0.6–10 MeV. For one bright burst, a time dependent spectral turnover was observed at MeV energies.

There is some evidence, in a single 6 s spectrum of GRB 910425, for an excessive soft component between 300 and 450 keV. Further studies are being carried out to determine the origin of this feature.

The COMPTEL images of GRBs and their intersection with triangulation arcs, determine the region of sky to be searched for quiescent GRB counterparts at other wavelengths. The good agreement between these independent methods also provides an impetus to pursue the rapid response campaign (Kippen et al. 1993) for rapid, multi-wavelength searches for fading counterparts to GRBs, using COMPTEL locations obtained within hours of the occurrence of the gamma–ray burst.

Acknowledgements. L.H. wishes to acknowledge an ESA fellowship. We are grateful to G. Fishman, K. Hurley, C. Kouvelioutou, M. Sommer, J. Laros, E. Fenimore and R. Klebesadel for communicating the 3^{rd} Interplanetary Network localisations of gamma–ray bursts prior to final publication

References

Barat, C., 1993, A&AS, 97, No. 1, 43
Baring, M.G., 1993, Proceedings of IAU Symposium No. 142
de Boer, H., Bennett, K., Bloemen, H., et al., 1992, The GRO Mission. In: Di Gesù, V., Scarsi, L., Buccheri, R., Crane, P., Maccarone, M., Zimmerman, H.U. (eds.) Data Analysis in Astronomy IV, Plenum, New York, p. 241
Cline, T.L., Hurley, K., Sommer, M., et al., 1993, Proceedings of the Compton Symposium, St. Louis, in press
Cline, T.L., Hurley, K.C., Boer, M., et al., 1992, Spatial and Intensity Distributions; Locations. In: Paciesas, W.S. & Fishman, G.J. (eds.) AIP Conference Proceedings 265, New York, p. 72
Cline, T.L., 1984, High Energy Transients in Astrophysics. In: Woosley, S.E. (ed.) AIP Conference Proceedings 115, New York, p. 333
Collmar, W., Bennett, K., Bloemen, H., et al., 1993, A&AS, 97, No. 1, 71
Connors, A., Aarts, H.J.M., Bennett, K., et al., 1993, A&AS, 97, No. 1, 75
Golenetskii, S.V., Mazets, E.P., Aptekar, R.L., Ilyinskii, V.N., 1983, Nature, 306, 451
Greiner, J., Wenzel, W., Hudec, R., et al., 1993, Proceedings of the Compton Symposium, St. Louis, in press
Harding, A.K., Petrosian, V., & Bussard, R.W., 1986, Spectra and Emission Mechanisms. In: Liang, E.P. & Petrosian, V. (eds.) AIP Conference Proceedings 141, New York, p. 128
Hurley, K., Boer, M., Sommer, M., et al., 1992a, Gamma–Ray Bursts. In: Shrader, C.R., Gehrels, N. & Dennis, B. (eds.) The Compton Observatory Science Workshop, NASA Conference Publication 3137, p. 288
Hurley, K., Kargatis, V., Liang, E., et al., 1992b, Spectral Observations. In: Paciesas, W.S. & Fishman, G.J. (eds.) AIP Conference Proceedings 265, New York, p. 195
Kippen, R.M., Macri, J., Ryan, J., McNamara, B., Meegan, C.A., 1993, Proceedings of the Compton Symposium, St. Louis, in press
Kwok, P.W., Bertsch, D.L., Dingus, B.L., et al., 1993, Proceedings of the Compton Symposium, St. Louis, in press
Lampton, M., Margon, B., & Bowyer, S., 1976, ApJ, 208, 177
Meegan, C.A., Fishman, G.J., Wilson, R.B., et al., 1992, Nature, 355, 143
Mitrofanov, I., Atteia, J.-L., Barat, C., et al., 1990, Observations. In: Ho, C., Epstein, R.I., Fenimore, E.E. (eds.) Gamma–Ray Bursts, Observations, Analyses and Theories, p. 209
Mitrofanov, I.G., Kozlenkov, A.A., Chernenko, A.M., et al., 1992, Spectral Observations. In: Paciesas, W.S. & Fishman, G.J. (eds.) AIP Conference Proceedings 265, New York, p. 163
Norris, J.P., Share, G.H., Messina, D.C., et al., 1986, ApJ, 301, 213
Pelaez, F., Bouchet, L., Jourdain, E., et al., 1993, Proceedings of the INTEGRAL Workshop, Les Diablerets
Schaefer, B.E., Teegarden, B.J., Cline, T.L., et al., 1992, ApJ, 393, L51
Schaefer, B.E., 1993, ApJ, 404, L87
Schmidt, W.K.H. 1978, Nature, 271, 525
Schneid, E.J., Bertsch, D.L., Fichtel, C.E., et al., 1992, A&A, 255, L13
Schönfelder, V., et al., 1984, IEEE Trans. Nucl. Sci. NS-31, 766
Schönfelder, V., et al., 1993, ApJS, 86, 657
Share, G.H., Johnson, W.N., Kinzer, R.L., et al., 1992, General, Historical, Recent Spacecraft Observations. In: Paciesas, W.S. & Fishman, G.J. (eds.) AIP Conference Proceedings 265, New York, p. 32
Varendorff, M.G., Bennett, K., de Boer, H., et al., 1992, Spatial and Intensity Distributions; Locations. In: Paciesas, W.S. & Fishman, G.J. (eds.) AIP Conference Proceedings 265, New York, p. 77

Vedrenne, G., 1981, Phil. Trans. R. Soc. Lond., A 301, 645
Winkler, C., Schönfelder, V., Diehl, R., et al., 1986, Adv. Space Res., Vol. 6 , No. 4, 113
Winkler, C., Bennett, K., Bloemen, H., et al., 1992a, A&A, 255, L9-L12
Winkler, C., Bennett, K., Bloemen, H., et al., 1992b, Proceedings of the Compton Symposium, St. Louis, in press

This article was processed by the author using Springer-Verlag LaTeX A&A style file version 3.